Scattering methods:

Structure and Dynamics on the Colloidal Length Scale

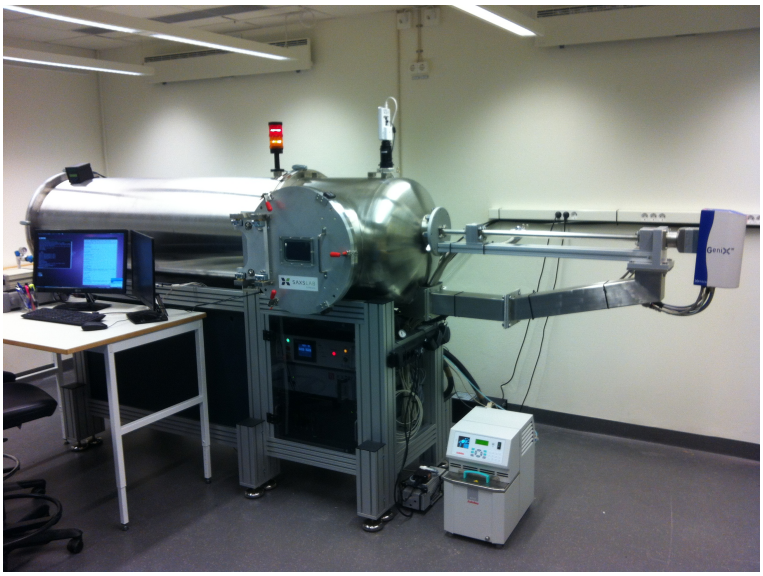

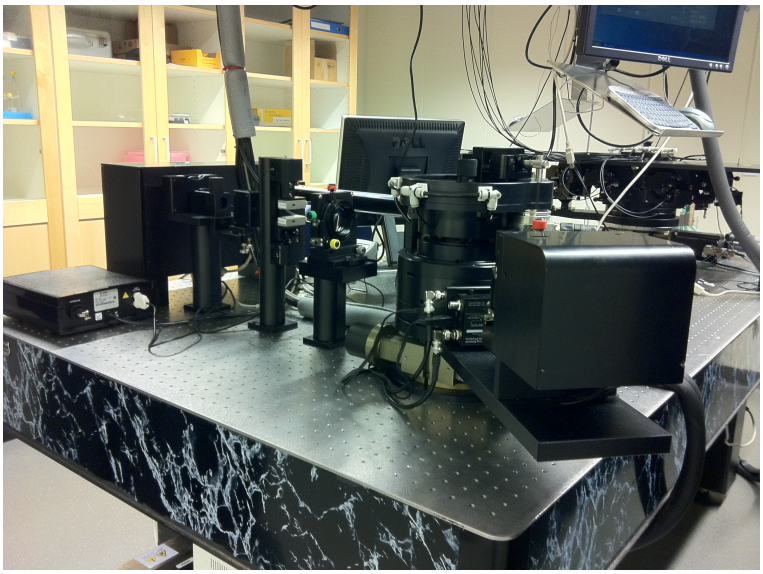

Ulf Olsson

2013

1. General background

Light that interacts with matter can be either absorbed and/or scattered. The latter is a prerequisite for our ability to see, and combined with absorption phenomena, enables color vision. In a more general sense, there are essentially two ways by which we can "see", if by seeing we mean determining the size and the shape of objects. The first, and most commonly known way to see, we may refer to as imaging. Here, by the use of a lens, the light that is reflected or scattered from an object is focused to create an image of the object on a screen. This is in principal how our eyes work. The light is focused by our eye lenses, sometimes in combination with glasses when the eye lenses are not operating properly, to create an image on the retina in the back of the eye, which is then analyzed by the brain. The second way to "see", we call scattering or diffraction. Here, we work without the focusing lens and instead measure and analyze the scattered intensity as a function of the scattering angle, θ, as illustrated schematically in Figure 1.

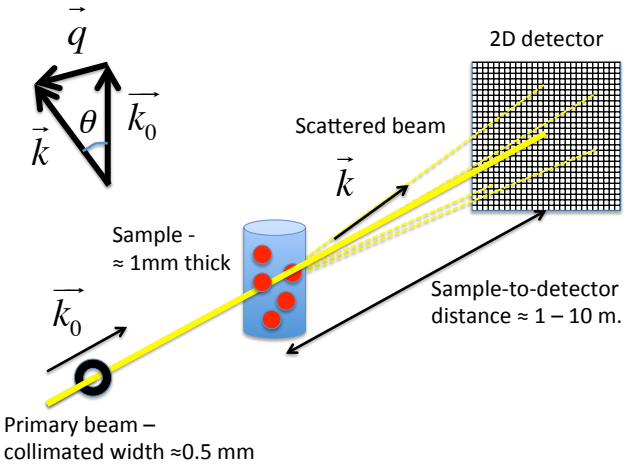

Figure 1. Schematic illustration of a (small angle) scattering experiment. An incoming primary beam, with wave vector $\vec{k}_0$, impact on a sample and the scattered radiation (wave vector $\vec{k}$) is here recorded by a two dimensional detector. The scattering vector, $\vec{q} = \vec{k} - \overrightarrow{k_0}$, is also illustrated.

The scattered intensity, $I(q)$, is generally presented, not as a function of the scattering angle, but as a function of the so called scattering vector (magnitude) $q = |\vec{q}|$, where $\vec{q} = \vec{k} - \overrightarrow{k_0}$ (see Figure 1) is the difference between the wave vectors of the scattered ($\vec{k}$) and incident ($\overrightarrow{k_0}$) beams, respectively. If the

scattering event is purely elastic, $|\vec{k}| = |\overrightarrow{k_0}| = \frac{2\pi}{\lambda}$, where λ is the wavelength of the radiation, the scattering vector magnitude is related to the scattering angle through

$$q = \frac{4\pi}{\lambda} \sin\frac{\theta}{2} \qquad (1)$$

In a scattering or diffraction experiment[1], a scattering or diffraction pattern is obtained that carries the information about object's size and shape, the number or concentration of objects and how the objects are distributed in space. A common and simple demonstration of the phenomenon, which can be found in general physics textbooks, is the diffraction from a thin slit, illustrated in Figure 2. A laser beam passing through a thin slit gets diffracted, and a characteristic diffraction pattern can be obtained on a screen behind the slit. This pattern consists of intensity maxima and minima, where the exact pattern (angles or q-values of maxima and minima) depends on the slit width.

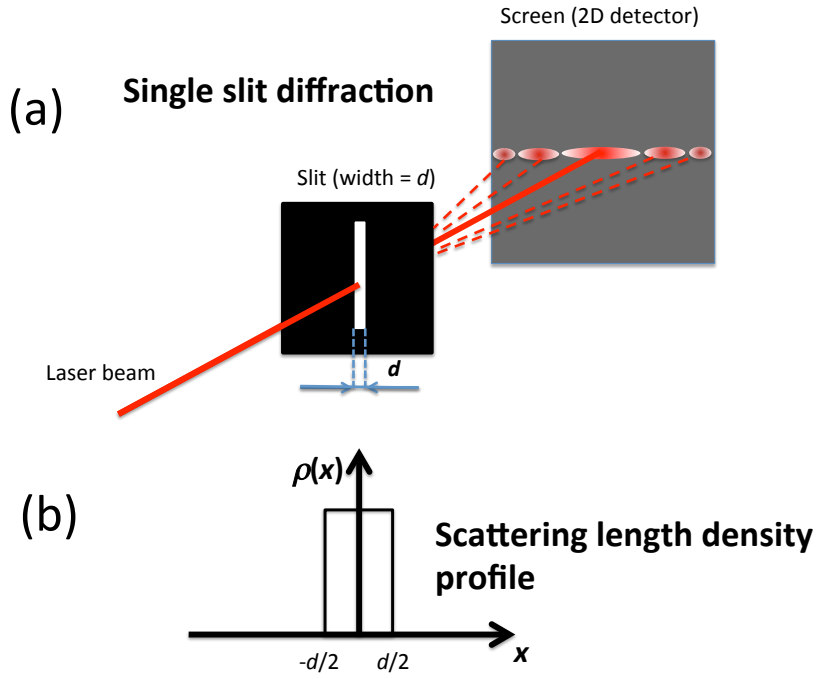

Figure 2. (a) Illustration of the single slit diffraction experiment. Note that diffraction is mainly observed perpendicular to the thin slit.
(b) The slit example corresponds to a rectangular scattering length density profile.

[1] The word diffraction is mainly used when the experiment is carried out on crystalline solids to obtain the crystalline structure, while the word scattering is mainly used for the analysis of the more diffuse scattering from liquids or amorphous objects.

The radiation is scattered by atoms and/or molecules, where different atoms/molecules have different scattering power. This result in a scattering contrast between different molecules, like between a polymer and a solvent, or between domains of different composition like in an emulsion, or in an aerosol. The scattering pattern, $I_{sc}(q)$, is related to the real space structure through a Fourier transform. We may illustrate this by the single slit diffraction in Figure 2, as the calculation here is relatively simple. Consider a long vertical, but narrow, slit. Because it is long in the vertical direction it scatters mainly in the horizontal direction (as will be explained below) and we only need to consider one dimension, the *x* direction. There is a finite scattering power only inside the slit. Outside the slit the beam is blocked and scattering power is zero. Denoting the scattering power by ρ, its variation in the *x*-direction, the scattering power profile $\rho(x)$, is illustrated in Figure 2 b, where *d* is the slit width. In this example the profile is rectangular with $\rho(x)=\rho_0$ inside the slit, and $\rho(x)=0$ elsewhere. The scattered intensity is now given by

$$I_{sc}(q) = \left|\int_{-\infty}^{\infty} dx\ \varrho(x)\ e^{iqx}\right|^2 = \varrho_0^2 \left|\int_{-d/2}^{d/2} dx\ e^{iqx}\right|^2 \qquad (2)$$

This Fourier integral has a relatively simple solution. We recall that $e^{i\theta} = \cos\theta + i\sin\theta$. Since the integration interval is even, the integral over the imaginary part vanishes, as the sine function is an odd function. Eq. (2) can thus be written as

$$I_{sc}(q) = \varrho_0^2 \left|\int_{-d/2}^{d/2} dx \cos qx\right|^2 = 4\varrho_0^2 \left(\frac{\sin\{qd/2\}}{q}\right)^2 \qquad (3)$$

This particular scattering pattern has zero intensity at $q=2\pi/d$, $4\pi/d$, $6\pi/d$,… and intensity maxima at $q=0$ and at $3\pi/d$, $5\pi/d$, $7\pi/d$,…, and where the intensity of the maxima decays as q^{-2}. From, for example, determining the *q*-value(s) where the intensity is zero or has a maximum we can obtain the slit width. In practice, this is done by measuring the corresponding scattering angles and knowing the wavelength of the light source. We see from Eq. (3) that as δ increases, the positions of the zeros move to lower *q*-values. In the limit of $d \to \infty$ all the zeros move into $q=0$. This means there is no scattering. Mathematically, this situation is described by $\int_{-\infty}^{\infty} dx\ e^{iqx} = \delta(0)$, where $\delta(x)$ is the Dirac delta function. Scattering only in the forward direction, $q=0$, is equivalent to a propagating beam (no scattering), and this is why we essentially do not see any vertical scattering from the slit when the slit length is large.

There is a fundamental condition that needs to be fulfilled in order to be able to "see" the shape and size of objects. This condition, which holds both for "seeing" by imaging or by scattering, is that the wavelength, λ, of the radiation used to "see" with, has to be smaller than the size of the object. This means that,

no matter how much we magnify, in a light microscope we cannot see objects that are smaller than a micrometer, which is approximately the wavelength of visible light. In order to "see" smaller things, the wavelength has to be made shorter. This is essentially no problem. Different sources with shorter wavelengths are available and there are also suitable detectors of such radiation, as we cannot use our eyes directly when we depart from the visible part of the spectrum. UV light is however not suitable for seeing. The reason is that essentially all matter absorbs rather strongly in UV, making all objects and matter dark. Decreasing the wavelength further into the so called X-ray regime, absorption decreases again and matter become increasingly transparent. While there still remains significant absorption, X-rays with $\lambda \approx 0.1$ nm (1 Å), is commonly used in scattering experiments.

This fundamental condition can also be illustrated by the help of Eq. (3). In order to determine the width of the slit we need to measure the q-value of at least the first intensity minimum occurring at $q=2\pi/d$. Since the maximum scattering angle is 180°, observing the first minimum requires $\lambda<2d$.

Besides X-rays, one can also produce electron and neutron beams with short wavelengths, suitable to see small things. For such particle beams the wavelength is related to the momentum, $p=mv$, through $\lambda=h/p$, where m is the mass, v the velocity and h is Plank's constant. A beam of charged electrons can be focused using electromagnetic lenses and are mainly used in electron microscopes. Neutrons can be produced with a suitable wavelength in reactors, or by so-called spallation, where protons are accelerated to high velocities and then impact on heavy atoms. In this spallation event, many neutrons are released. Neutrons are mainly used for scattering experiments and have some particular advantages compared to X-rays. For most materials absorption is negligible and neutrons can therefore penetrate deep into the materials. The scattering mechanism involves interactions with the atomic nuclei and the scattering power, and thus the contrast, can be varied by isotopic substitution. In particular substituting normal hydrogen with deuterium is often used to highlight certain parts of the molecule. On the other hand, X-rays are scattered by electrons and the atomic scattering power thus increases with the atomic number. Hydrogen, which has only one electron, is almost invisible to X-rays while it strongly scatters neutrons. Neutron scattering is therefore important for studies of hydrogen storing materials and to refine protein structures when hydrogen positions are important. Neutrons, being spin=1/2 particles, carry a magnetic moment and also are scattered by local magnetic fields inside materials which is used in the studies of high temperature superconductors.

Above we have discussed scattering experiments in general terms. For what remains we will focus on some particular scattering experiments that are commonly used to study colloids, gels, polymers, lipids proteins or other soft matter systems, with characteristic (colloidal) length scales in the range 1 nm - 1

μm. These are small angle scattering of X-rays or neutrons, and static and dynamic light scattering.

2. Small angle scattering

Scattering experiments probe the structure on the length scale $2\pi/q$. Hence, in order to investigate structures on the colloidal length scale we typically need access to the q-range 0.01 – 10 nm. With X-rays of wavelength 0.1 nm, this corresponds to small angles, 0.01° – 10°, as obtained using Eq. (1). When we are only interested in small angles a typical instrument design involves a narrowly collimated X-ray beam, produce by an X-ray source and giving a spot size of a fraction of a mm (≤ 0.5 mm) on a sample typically contained in a glass capillary of 1 mm in diameter. The scattered intensity is recorded by a stationary, typically a 2-dimensional area detector (*e.g.* a ccd camera), placed behind the sample, as illustrated in Figure 1. On the detector there is also a beamstop that protects the detector from the intense primary beam, and the whole or at least most of the system is kept under vacuum to avoid scattering from air that would result in a background noise. The available q-range depends on the diameter of detector, the diameter of the beamstop and sample-to-detector distance. Reaching very low q-values requires a very long sample-to-detector distance (several meters) and a narrow beam and beamstop, while larger q-values can be obtained by shortening the sample-to-detector distance. To cover a large q-range it is clearly advantageous to be able to vary the sample-to-detector distance. Alternatively, one sometimes uses two detectors simultaneously, one low angle and one wide angle detector. For a more detailed description see *e.g.* the review of Narayanan. [1]

From isotropic solutions or dispersions, the scattering pattern is circularly symmetric (Figure 3 left). This pattern is then usually radially averaged to produce the one dimensional scattering pattern I(q) vs. q (Figure 3 right). The intensity is a measure of the energy flux, *i.e.* the number of photons/particles, passing a unit area perpendicular to the propagation per unit time. The scattered intensity, I_{sc}, recorded by the detector depends on the intensity of the primary beam, I_0, on the irradiated sample volume, V_s, and on the sample-to-detector distance, $l_{s\text{-}d}$, parameters that vary from experiment to experiment. It is therefore useful to define an absolute intensity scale, where the experimentally recorded intensity is normalized with respect to these variables. I_{sc} is proportional to I_0 and V_s and because radiation intensities decay as the inverse square of the distance, the absolute scaled intensity is defined as

$$I = \frac{l_{s-d}^2}{I_0 V_s} I_{sc} \qquad (4)$$

In terms of a wave description of the radiation, $A(x) = A_0 \cos(x)$, the intensity is given by the square of the amplitude, $I = |A_0|^2$, which is the reason for the square in Eqs. (2) and (3). To obtain the experimental scattering data on absolute scale one typically do a calibration with a known scatterer. In the case of X-rays one often chose pure water.

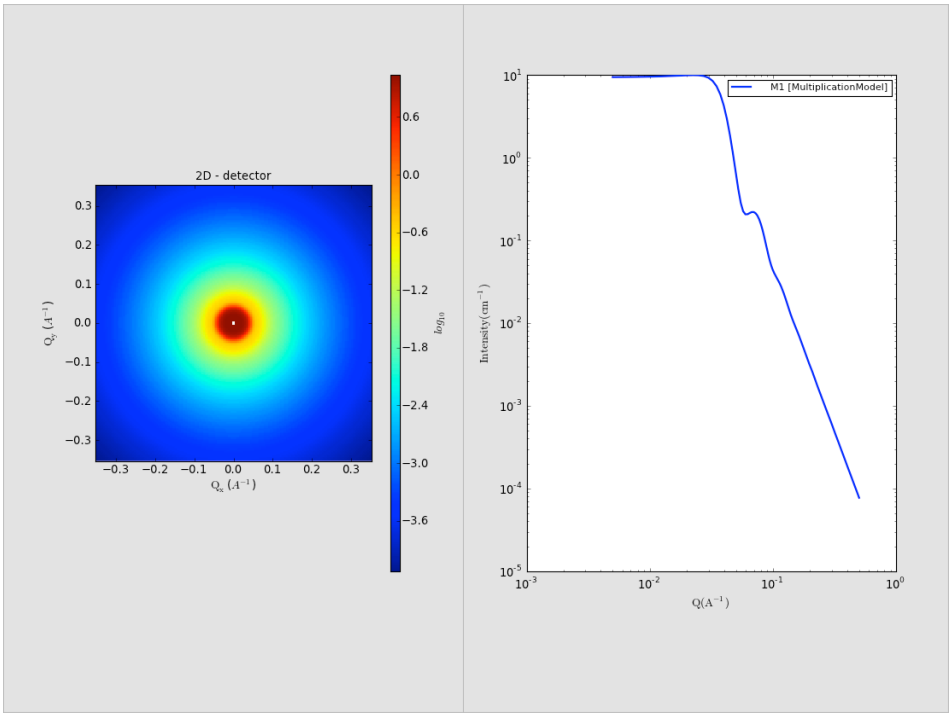

Figure 3. (Left) typical two dimensional small angle X-ray scattering pattern from a dispersion of spherical colloidal particles. (Right) Radially averaged scattered intensity, I(q), plotted as a function of q.

Turning now to the scattering from colloidal particles, we consider first a single spherical colloidal particle in vacuum. This can save as an example of aerosols or the ice-particles of the clouds in the sky, if we neglect the scattering from the air molecules. The single particle scattering function is given by the square of a Fourier integral, as in the example of the slit in Eqs. (2) and (3). Now, however we have to integrate over a sphere in three dimensions, with the position/coordinate vector $\vec{r} = (x, y, z)$. If $\rho(x)$=ρ_p inside the sphere while being zero elsewhere $I(q)$ for the sphere is given by

$$I_{sc}(q) \sim \varrho^2 V_s^2 \left(\frac{3(sin(qR) - qRcos(qR))}{(qR)^3} \right)^2 \qquad (5)$$

where R is the sphere radius and V_s=4πR^3/3 is the sphere volume. If the particle surrounding is not vacuum but for example a solvent then ρ in Eq. (5) should replaced by $\Delta\rho$, the difference in ρ between the particle and the solvent. Strictly, ρ has the dimension of length^{-2}, *e.g.* cm^{-2}. It is often referred to as the scattering

length density, and $\Delta\rho$ is the contrast between the particle and the surrounding solvent. If $\Delta\rho$=0, the particle is "invisible". X-rays are scattered by individual electrons and for this type of radiation, ρ is proportional to the electron density of the material and X-ray contrast is obtained by differences in electron density.

The q dependence of Eq. (5) is given by the function

$$P(q) = \left(\frac{3(sin(qR) - qRcos(qR))}{(qR)^3}\right)^2 \qquad (6)$$

$P(q)$ is referred to as the (normalized) particle formfactor, and it is this part that carries the information of the particle shape, here a homogeneous sphere. $P(q)$ is normalized, so that in the limit in of q=0, $P(0)$=1. For cylindrical or disc shaped objects, this function is different. Also, if the particle is not homogeneous, but, for example, is hollow, consisting of a spherical shell, as for a lipid vesicle, $P(q)$ is significantly different. A library of form factors can be found in the review by Pedersen [2].

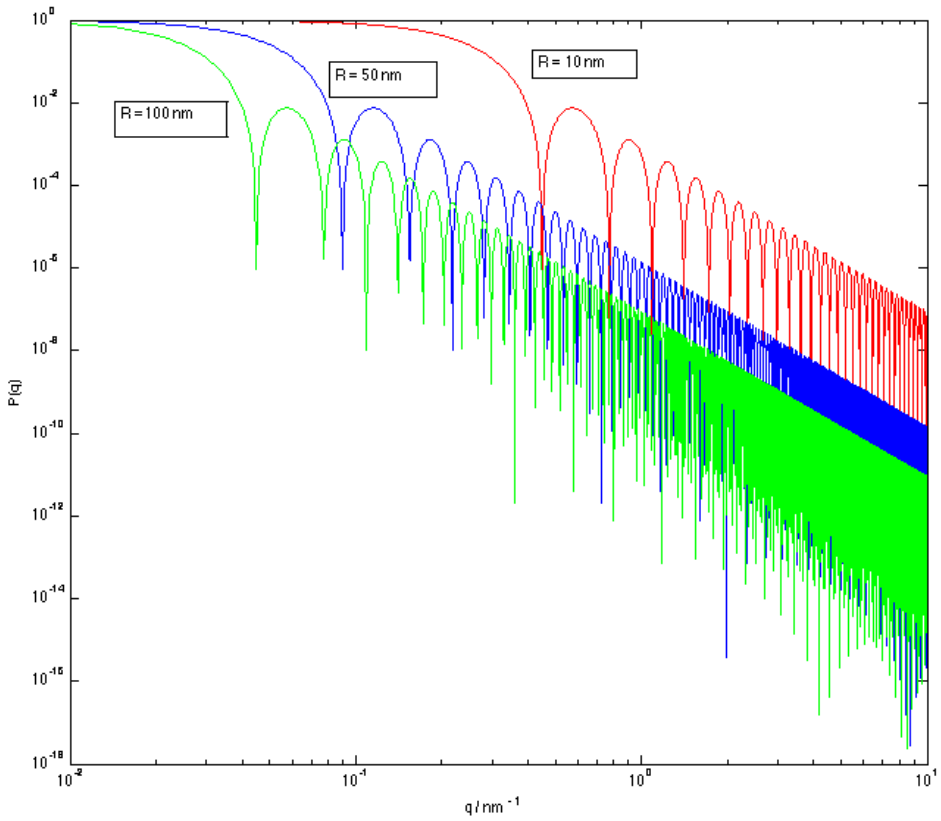

Figure 4. $P(q)$ for homogeneous spheres of radii R=10, 50 and 100 nm, respectively.

$P(q)$ for homogeneous spheres of radii R=10, 50 and 100 nm, respectively, are presented in Figure 4, in a double logarithmic plot. The normalized $P(q)$ begins at 1 at q=0 and then decays with increasing q showing also oscillations due the sine and cosine functions (Eq. (6)). The particular pattern of maxima and

minima reports on the particles shape. The alternating maxima and minima (zeros) shift to lower q with increasing R.

Typical scattering experiments are performed on solutions or dispersions with a large number of particles in the scattering volume. When they are dilute, with average nearest neighbor distance being much longer than R, the total scattering will just be the sum of the scattering from the different particles. At higher concentrations, however, the scattered intensity will also depend on the structure formed by the particles in the solution, a consequence of inter-particle interactions. In contrast to crystals, however, where the structure is long-range, the structure in solutions is only short-range. The effect is accounted for by multiplying with the so-called structure factor, $S(q)$, so that our final expression for the absolute scaled scattered intensity is

$$I(q) = \frac{N_p}{V} V_p^2 \Delta\varrho^2 P(q) S(q) \qquad (7)$$

where N_p/V is the number density of particles, V_p is the particle volume, $P(q)$ is the normalized form factor and $S(q)$ is the structure factor. $P(q)$ and $S(q)$ are dimensionless and we then see in Eq. (7) that $I(q)$ has the dimension of inverse length.

In statistical mechanics, the structure of liquids is generally described in terms of the radial distribution function, $g(r)$, that tells the probability of finding another particle (or the average particle concentration) at a distance r from a given test particle. $S(q)$ is the Fourier transform of $g(r)$ and thus carry the same information about the structure, but in the reciprocal space. From the value of structure factor in the limit of q=0, we can obtain the osmotic compressibility of the sample

$$S(0) = k_B T \left(V_p \frac{\partial \pi}{\partial \phi} \right)^{-1} \qquad (8)$$

as a measure of the inter particle interactions. Here, π is the osmotic pressure, and ϕ is the volume fraction of particles.

In Figure 5 we have plotted S(q) as a function of qR for some different concentrations of spherical particles interacting as hard spheres. For this case there exists and analytical expression that for example can be found in [3]. At low concentrations the particles are essentially non-interacting and the solutions behave as ideal with $\pi=\phi k_B T/V_p$, and $S(q)\approx 1$ for all q-values. With increasing concentration the excluded volume interactions of the hard spheres become significant and the solution becomes increasingly structured, as seen by the oscillations in $S(q)$ and the decreased osmotic compressibility.

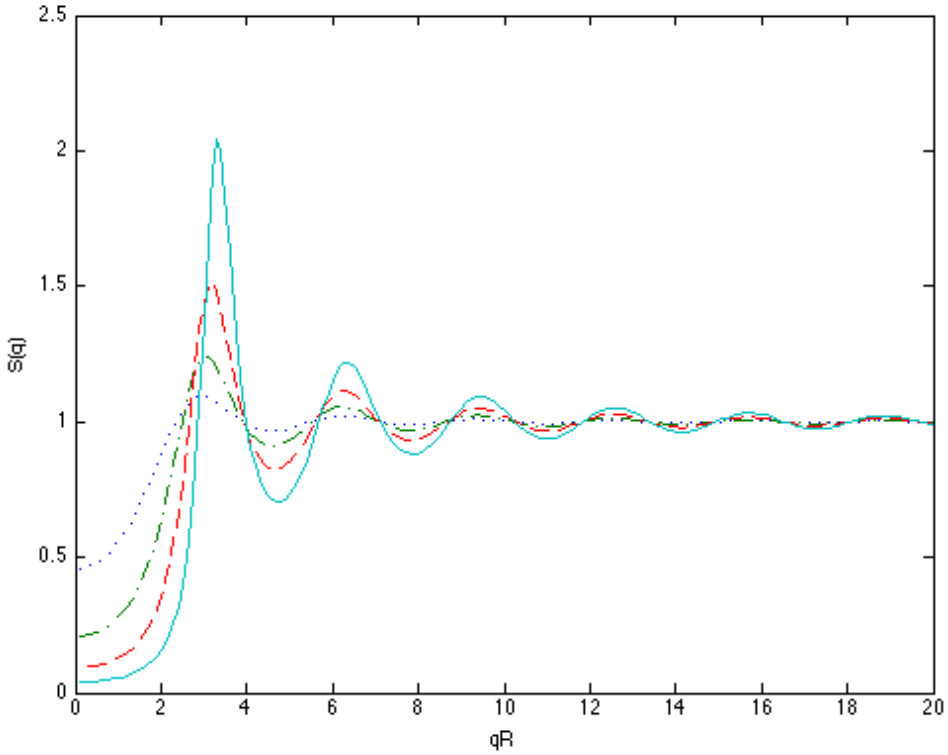

Figure 5. $S(q)$ plotted as a function of qR for some different concentrations of spherical particles interacting as hard spheres. Dotted line: ϕ=0.1, dashed dotted line: ϕ=0.2, dashed line: ϕ=0.3, and solid line: ϕ=0.4. The correlation peak moves to higher q with increasing concentration as the average separation between particles decreases.

In Figures 6-8 we have plotted separately $P(q)$ (upper left), $S(q)$ (upper right) and $I(q)$ (bottom left (linear scale) and right (log-log scale)) for a hard sphere system with volume fractions ϕ=0.01, 0.10 and 0.40, respectively. In the bottom right figure, $I(q)$ (solid blue line) is compared with $P(q)$ (broken green line). As can be seen, there is an increased influence of the structure factor on the scattering pattern as concentration increases. At the lowest concentration ϕ=0.01 (Figure 6) $S(q)\approx 1$ and does not influence the scattering significantly.

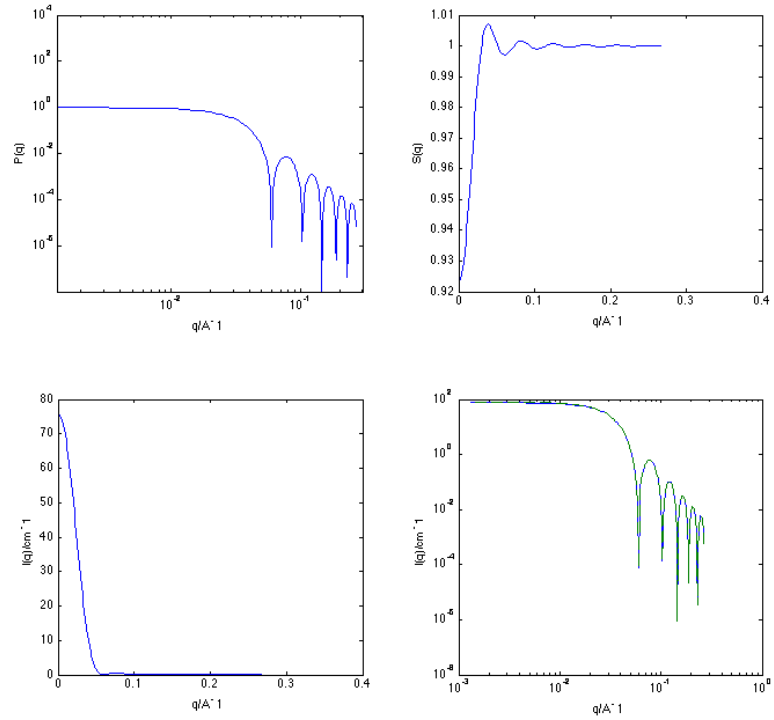

Figure 6. $P(q)$ (upper left), $S(q)$ (upper right) and $I(q)$ for a dispersion of spherical homogeneous hard sphere particles of R=10 nm and ϕ=0.01.

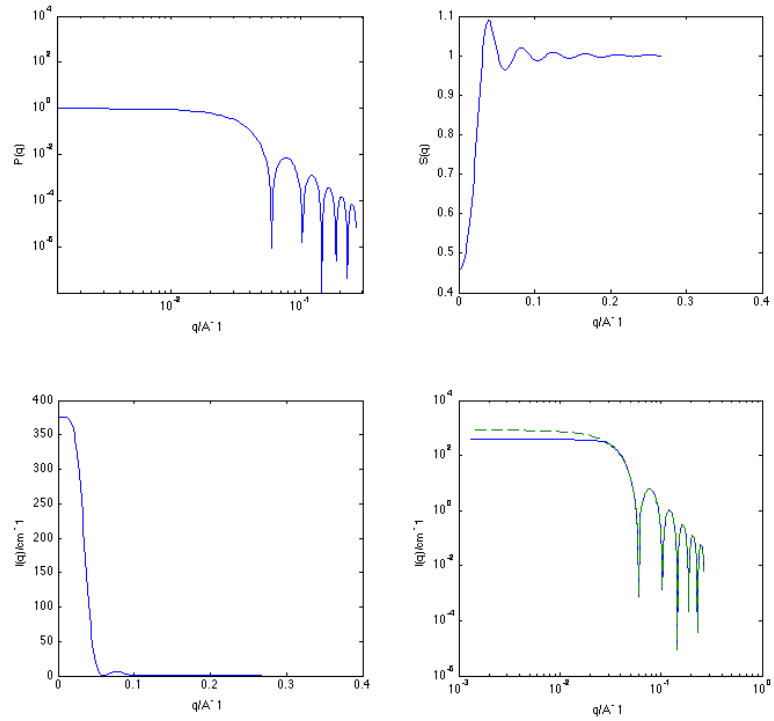

Figure 7. $P(q)$ (upper left), $S(q)$ (upper right) and $I(q)$ for a dispersion of spherical homogeneous hard sphere particles of R=10 nm and ϕ=0.10.

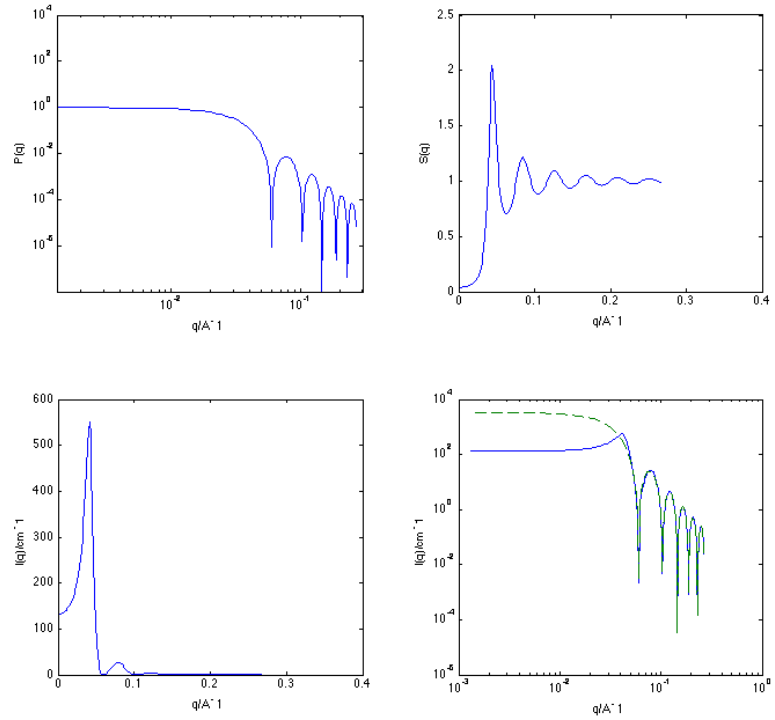

Figure 8. $P(q)$ (upper left), $S(q)$ (upper right) and $I(q)$ for a dispersion of spherical homogeneous hard sphere particles of R=10 nm and ϕ=0.40.

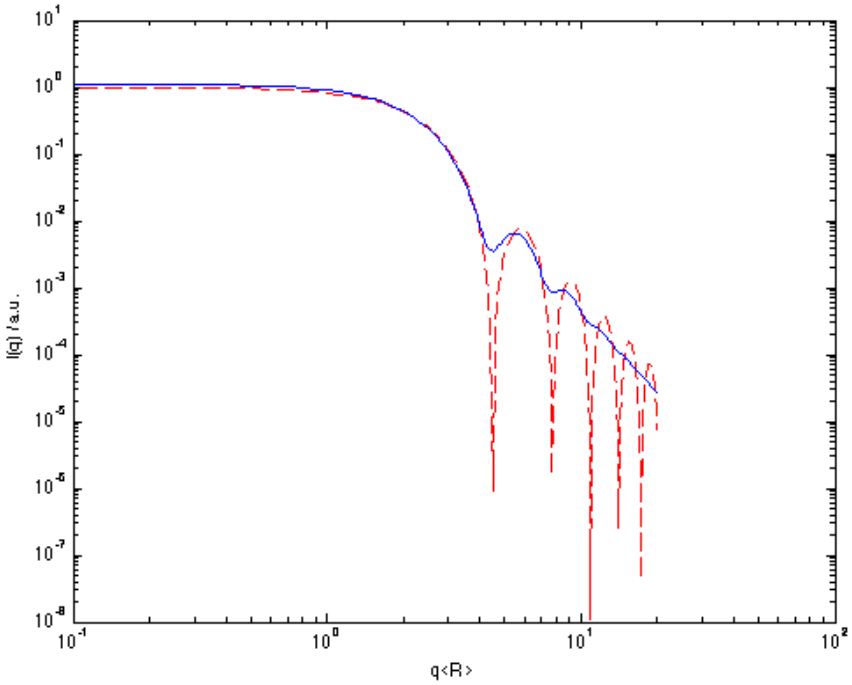

Figure 9. Comparison of $P(q)$ for monodiperse spheres with R=10 nm (red dashed line) with the average $P(q)$ for polydisperse spheres with $\langle R \rangle$=10 nm and relative standard deviation $\sigma/\langle R \rangle$=0.10 (blue solid line). Polydispersity removes the formfactor minima in the scattering pattern.

Up to now we have only considered monodisperse particles, *i.e.* where all particles have exactly the same size. This is seldom the case in reality. Most often there is a mixture of sizes, with a size distribution that for example can be Gaussian $N_p(R)/V \sim exp\{(R-\langle R\rangle)^2/2\sigma^2\}$, where $N_p(R)/V$ is the concentration of particles with radius R, and the distribution is characterized by a mean value <*R*> and a standard deviation, σ. The main effect of the polydispersity is that the formfactor minima in the scattering patters become less distinct as the different particle sizes have their minima at different q values. In Figure 9 we compare $P(q)$ from monodisperse spheres of with and average $P(q)$ from a system with a Gaussian distribution of sizes with a relative standard deviationσ/<*R*>=0.1. With this polydispersity only the first two minima are clearly visible.

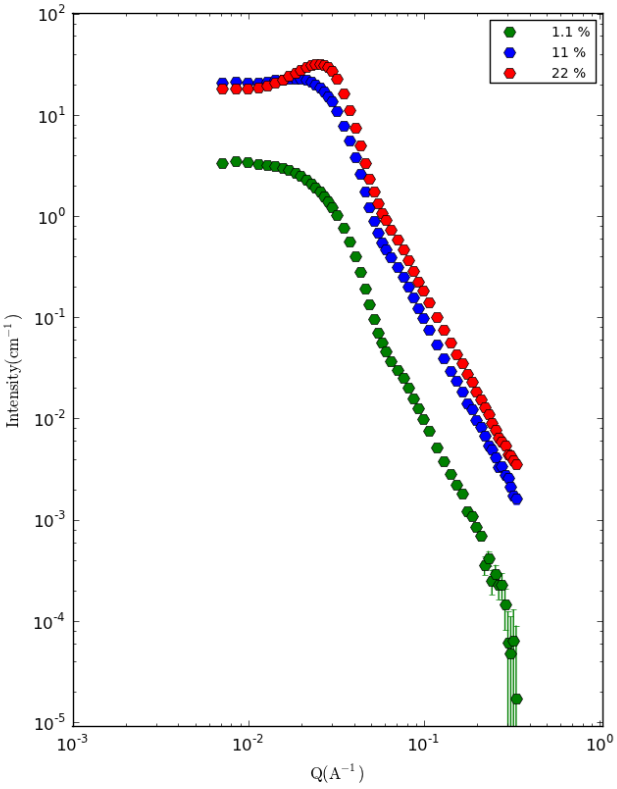

Figure 10. SAXS data from aqueous solutions of microemulsion oil-droplets with radius R≈8 nm. Data from reference [4]. The oil (decane) droplets are covered and stabilized by a layer of the nonionic surfactant $C_{12}E_5$, and interact to a good approximation as hard spheres. Three different concentrations are shown, ϕ=0.011, 0.11 and 0.22, respectively.

In Figure 10 we show the scattered intensity from a real experimental system. The data were recorded in SAXS experiments and the system is a microemulsion where spherical droplets of decane, covered by a stabilizing layer

of the nonionic surfactant $C_{12}E_5$ (penta ethyleneglycol dodecyl ether), are solubilized in water. The mean radius of these microemulsion droplets is 8 nm and $\sigma/\langle R\rangle \approx 0.15$.[4] The scattering from three different concentrations, ϕ=0.011, 0.11 and 0.22, respectively, are shown. The scattered intensity at higher q, where $S(q)\approx 1$ for all concentrations, is proportional to ϕ. At lower q, the structure factor reduce the scattered intensity for higher concentrations. Below we will also discuss light scattering from the same microemulsion system.

Finally in this section we note that Eq. (7) also states that there is very strong dependence of the scattered intensity on the particle size. For a given volume fraction of particles, $\phi = N_p V_p / V$, the scattered intensity is proportional to the particle volume which, in the case of homogeneous spheres, means a proportionality to R^3. Air and water molecules scatter the sunlight only little and the main effect is the blue color of the sky. When water molecules in humid air condense to form droplets and ice particles, they scatter much more, and the resulting clouds are clearly visible. The blue color of the sky is a consequence of the particularly strong wave length dependence of scattering of visible light, as will be discussed further in the next section.

3. Static Light Scattering.

With visible light we have access to small q-values. Mostly, the wavelength of the light (ca. 500 nm) is longer than the size of the particles we are studying. In this case, we will not see any formfactor minima within the accessible q-range (for a homogeneous sphere, the first formfactor minimum occurs at $q = 4.5/R$). Rather, we only see the low q part of the product $P(q)S(q)$. With light scattering experiments we can make accurate extrapolations to q=0 to determine properties like V_p (the molecular weight of polymers is often determined this way) and $(\partial\pi/\partial\phi)^{-1}$, but we are typically unable to determine the particle shape. While we will not detect any formfactor minima, the monotonic variation (decay) of $I(q)$ with q can still be evaluated, to obtain the radius of gyration, R_g, from the leading term in the series expansion of $P(q)$

$$P(q) = 1 - \frac{q^2 R_g^2}{3} + \ldots \qquad (9)$$

For a homogeneous sphere, $R_g = (3/5)^{1/2} R$.

In light scattering experiments one often explores a wide range of scattering angles (15° – 165°). A schematic description of a light scattering setup is shown in Figure 11. A laser beam is focused on the sample and the scattered light is collected by, for example, a photo diode placed on a movable arm (goniometer), to detect the scattering at different angles. The laser wavelength (*e.g.* 633 nm for a Helium-Neon laser) is generally expressed as the wavelength in vacuum. In the sample, this wavelength becomes λ/n, where n is the refractive

index of the solution, and the expression for the q-vector is, for light scattering, generally written

$$q = \frac{4\pi n}{\lambda} \sin\frac{\theta}{2} \qquad (10)$$

With a He-Ne laser the accessible q-range becomes ca. 0.0035 – 0.026 nm^{-1} in water (n=1.33). In light scattering, the absolute scale scattered intensity is generally referred to as the excess Rayleigh ratio, $\Delta R(q)$. The data are converted into absolute intensities using

$$\Delta R(q) = \frac{\Delta I(q)}{I_{ref}(q)} \left(\frac{n}{n_{ref}}\right)^2 R_{ref}(q) \qquad (11)$$

Here, $\Delta I_{ref}(q)$ is the excess scattered intensity of the sample, where the scattering from the solvent and sample tube has been subtracted, and n its refractive index. $I_{ref}(q)$ is the scattered intensity of the reference solvent and n_{ref} its refractive index. R_{ref} is the Rayleigh ratio of the reference solvent. A common solvent for absolute scale calibration of the scattered intensity is toluene.

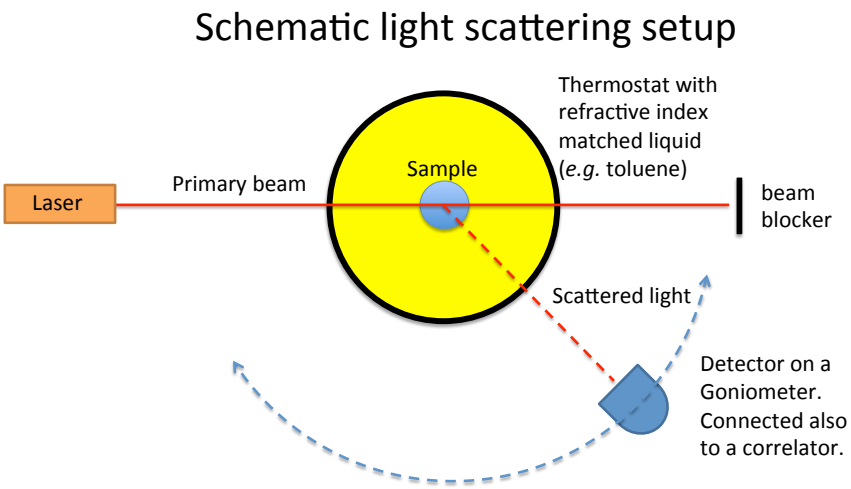

Figure 11. Schematic outline of a typical goniometer light scattering instrument. A laser beam of 1-2 mm width shines on a sample inserted in a liquid (often toluene or decaline) having a refractive index very close to that of the sample container (glass) to minimize reflections etc. The index matched liquid is also used as a thermostat. The scattered light is recoded by a detector (*e.g.* photo diode), fixed on a goniometer arm. For dynamic light scattering experiments, intensity correlations are analyzed in a correlator.

The contrast comes from the difference in the refractive index between particle and solvent. In light scattering this is quantified in terms of the so-called refractive index increment, $dn/d\phi$ (more commonly expressed as dn/dc, where c is the molar concentration).

The light scattering power of molecules depends on their polarizability, which is linked to the refractive index. The scattered light intensity has a very strong wavelength dependence, $I \sim \lambda^{-4}$. This is the reason why the sky is blue (on a sunny day). When we look at the sky, we detect photons from the white light of the sun that have been scattered by air molecules in the atmosphere. Blue photons (λ=400 nm) are scattered more frequently than other visible wavelengths and this is why the sky is blue. This is also why the sun looks yellow. Blue photons have preferentially been depleted from the originally white light and the result is that the transmitted sunlight is yellow. At sunset, the sun light takes a longer path through the atmosphere. As a consequence there is more scattering. Often, we then find that the sun looks beautifully red. This is because so much of the other colors have been scattered, that only the longest wavelength (800 nm) has a significant transmission. This is helped if the atmosphere also is polluted by soot or other particles.

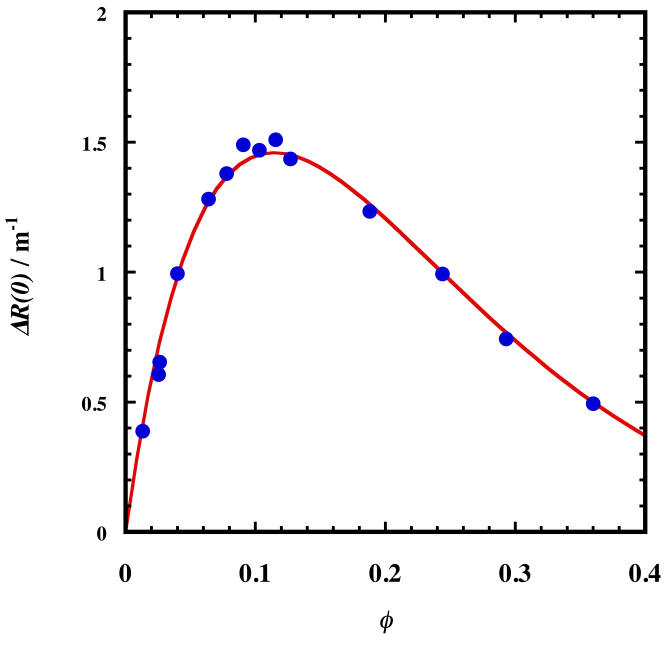

Figure 12. The excess Rayleigh ratio extrapolated to q=0, plotted as a function of the volume fraction for the same water-$C_{12}E_5$-decane microemulsion as in Figure 10. Data from reference [5] The solid line is the theoretical prediction for hard spheres.

The excess Rayleigh ratio can be expresses as

$$\Delta R(q) = \phi \frac{4\pi^2 n_0^2}{\lambda^4} \left(\frac{dn}{d\phi}\right)^2 V_p P(q) S(q) \qquad (12)$$

where n_0 is the refractive index of the solvent and n is the refractive index of the solution. Extrapolating data to q=0, where $P(q)$=1, we can, determine V_p if the solution is dilute so that also $S(q)$=1. As mentioned above, this is commonly done to determine the molecular weight of polymers. If V_p, on the other hand, is known from other measurements, $\Delta R(0)$ determined as a function of ϕ reports on interparticle interactions via the concentration dependence of $S(0)$. Figure 12 shows the variation of $\Delta R(0)$ with ϕ in a microemulsion composed of spherical oil droplets (R= 8 nm) in water, covered and stabilized by a layer of nonionic surfactant. [5] The system is in fact the same as in the SAXS study discussed above (Figure 10). The solid line is the prediction for hard spheres, given by the Carnahan-Starling equation. [6] At lower concentrations the intensity increases with concentration because of the increased number of particles. At higher concentrations, however, the scattered intensity decreases because of the repulsive interactions. This has a very important consequence. Our eye lenses are composed of concentrated ($\phi \approx 0.3$) protein solutions. For obvious reasons they need to be transparent, with only very low scattering of light. This is secured by the strong, here electrostatic, repulsions between the protein molecules. In the cataract disease, the eye lens has turned turbid with significant light scattering. This is because for some of the proteins interactions have shifted from net repulsive to attractive and the proteins have aggregated into larger objects. [7]

4. Dynamic light scattering.

The scattered intensity measured in static light scattering experiments corresponds to a time average, $<I(q)>$. The fluctuations of the intensity arise because the relative positions of all the particles are constantly changing as they undergo Brownian motion. The static structure factor, discussed above, is therefore strictly a time average. Fluctuations in the intensity may also arise from particle shape fluctuations, *i.e.* fluctuations in $P(q)$, but this can often be neglected, and will not be discussed further here. By analyzing the rate of intensity fluctuations we get information about the rate of particle motions. In a dynamic light scattering experiment the autocorrelation function of the intensity fluctuations is recorded. This is done recording the intensity at different times, multiply those values with the value at t=0, repeat this operations many times and finally take the statistical average of the products to form the autocorrelation function, $G(t) = \langle I(0)I(t)\rangle$. Here, $\langle \quad \rangle$ symbolizes that it is an average. This correlation function has the value $\langle I^2 \rangle$ at t=0 and decays to $\langle I \rangle^2$ at

long times when $I(0)$ and $I(t)$ has become uncorrelated. Often one considers the modified correlation function $g_2(t)$-1, where $g_2(t)=G(t)/\langle I\rangle^2$. For the case of monodisperse particles this is an exponential

$$g_2(t) - 1 = Ae^{-2\Gamma t} \qquad (13)$$

where A is an instrumental constant the relaxation rate Γ is given by

$$\Gamma = D_c q^2 \qquad (14)$$

The q^2 dependence is indicative of diffusive motion and D_c is the collective diffusion coefficient. D_c depends on particle size, but also on interactions, direct as well as hydrodynamic. In dilute solutions where interactions can be neglected, we can obtain the hydrodynamic radius, R_H, from D_c that here equals the Stokes-Einstein diffusion coefficient

$$D_0 = \frac{k_B T}{6\pi\eta R_H} \qquad (15)$$

Here, k_B is Boltzmann's constant, T the absolute temperature and η the solvent viscosity. For hard sphere systems, D_0 has only a weak concentration dependence.

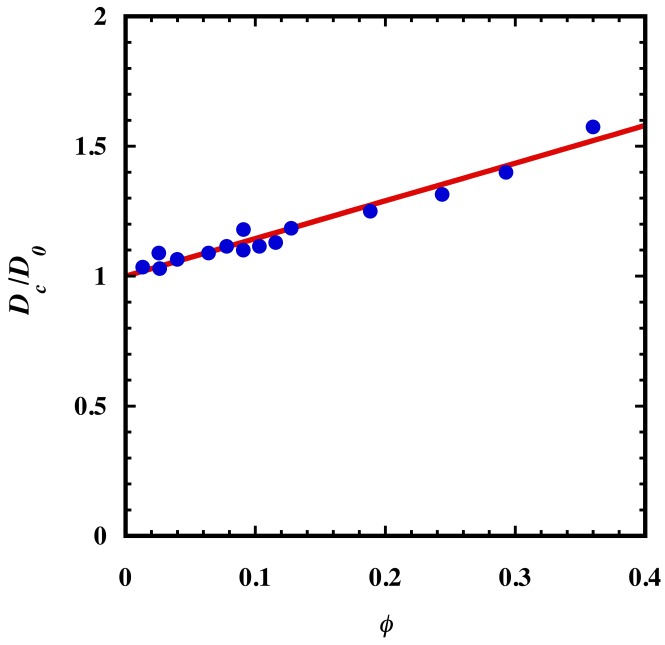

Figure 13. The relative collective diffusion coefficient, D_c/D_0, plotted as a function of the volume fraction for the same water-$C_{12}E_5$-decane microemulsion as in Figures 10 and 12. Data from reference [5]. D_0=2.0 10^{-11} m^2s^{-1}. The solid line is the theoretical prediction for hard spheres.

In Figure 13 we show the variation of D_c with concentration in the same nonionic microemulsion system as in the Figures 10 and 12.[5] The solid line is a theoretical prediction [8] for hard spheres, $D_c/D_0 = 1 + 1.45\phi$. From the value of D_c extrapolated to ϕ=0 (D_0=2.0 10^{-11} m^2s^{-1}), a hydrodynamic radius of ca. 90 nm is obtained, using Eq. (15).

References

(1) T. Narayanan *Curr. Opin. Colloid Interface Sci.* 2009, 14, 409
(2) J. S. Pedersen *Adv. Colloid Interface Sci.* 1997, 70, 171.
(3) D. J. Kinnig and E. L. Thomas *Macromolecules* 1984, 17, 1712.
(4) J. Balogh, U. Olsson and J. S. Pedersen *J. Disp. Sci. Tech.* 2006, 27, 497.
(5) U. Olsson and P. Schurtenberger *Langmuir* 1993, 9, 3389
(6) N. F. Carnahan and K. E. Starling *J. Chem. Phys.* 1969, 51, 635.
(7) A. Stradner, G. Foffi, N. Dorsaz, G. Thurston and P. Schurtenberger *Phys. Rev. Lett.* 2007, 99, 198103.
(8) P.N. Pusey in *Liquids, Freezing and the Glass Transition*, (Les Houches Session LI); Levesque, D., Hansen, J., Zinn-Justin, J., Eds.; Elsevier: Amsterdam, 1990